Chemico-Biological Interactions 381 (2023) 110570

Contents lists available at ScienceDirect

Chemico-Biological Interactions

journal homepage: www.elsevier.com/locate/chembioint

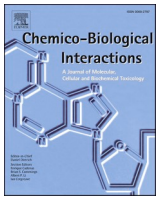

Research paper

Untargeted and targeted metabolomics reveal bile acid profile changes in rats with ethylene glycol-induced calcium oxalate nephrolithiasis

Zijian Zhou [a,1], Dexiang Feng [b,1], Donghui Shi [c,1], Peng Gao [a,d], Lujia Wang [a,d,*], Zhong Wu [a,d,**]

[a] Department of Urology, Huashan Hospital, Fudan University, Shanghai, 200040, PR China
[b] Department of Urology, Dushu Lake Hospital Affiliated to Soochow University, Medical Center of Soochow University, Suzhou Dushu Lake Hospital, Suzhou, 215123, PR China
[c] Department of Urology, Suzhou Wu Zhong People's Hospital, Suzhou, 215100, PR China
[d] Clinical Research Center of Urolithiasis, Shanghai Medical College, Fudan University, Shanghai, 200040, PR China

ARTICLE INFO

Keywords:
Nephrolithiasis
Calcium oxalate
Ethylene glycol
Metabolomics
Bile acid
Biomarker

ABSTRACT

Calcium oxalate (CaOx) nephrolithiasis is a prevalent disorder linked to metabolism. Examining metabolic alterations could potentially give an initial understanding of the origins of CaOx nephrolithiasis. This study aims to determine gut metabolic biomarkers differentiating CaOx nephrolithiasis utilizing untargeted and targeted metabolomics. CaOx nephrolithiasis model rats were built by 1% ethylene glycol administration. Histologic staining and renal function measurement revealed the presence of crystals in the lumen of the renal tubules, the renal injury and interstitial fibrosis in CaOx rats, demonstrating that the models of CaOx were established successfully. Hematoxylin & eosin (H&E) staining showed that CaOx group had inflammation and damage in the ileal tissue. Immunofluorescence and PCR results displayed that the tight junction proteins, ZO-1 and Occludin levels were decreased in the ileal tissues of the CaOx group. The untargeted metabolomic analysis revealed that 269 gut metabolites were differentially expressed between the CaOx group and the control group. Meanwhile, bile secretion, the main metabolic pathway in CaOx nephrolithiasis, was identified. Following, five significant bile acid metabolites were selected utilizing the targeted bile acid metabolomics, including Hyodeoxycholic acid (HDCA), Glycohyodeoxycholic acid (GHDCA), Nor-Deoxycholic Acid, omega-muricholic acid, and Taurolithocholic acid. Among these metabolites, HDCA and GHDCA presented the highest predictive accuracy with AUC = 1 to distinguish the CaOx group from the control group. As a result of network pharmacology, target genes of HDCA and GHDCA in CaOx nephrolithiasis were enriched in oxidative stress and apoptosis pathways. Conclusively, our study provides insight into bile acids metabolic changes related to CaOx nephrolithiasis. Although alterations in biochemical pathways indicate a complex pathology in CaOx rats, bile acid changes may serve as biomarkers of CaOx nephrolithiasis.

1. Introduction

Calcium oxalate (CaOx) nephrolithiasis is one of the most frequent pathologies of the urinary system with an ever-increasing prevalence [1]. It is thought to be a multifactorial disease involving metabolic disorders [2,3]. Current hypotheses propose that supersaturation and deposition of CaOx crystals in renal tissues contribute to kidney tubular cell apoptosis and injury, thus facilitating ongoing kidney stone formation [4]. Extensive studies have revealed that gut microbes can regulate this disease process via gut–kidney axis in CaOx nephrolithiasis [5–8]. Notably, metabolites are known to be a major form of communication between the host and the microbes [9]. Therefore, the role of metabolites in CaOx nephrolithiasis cannot be overlooked. One of the most abundant classes of metabolites, short-chain fatty acids (SCFAs), has been identified as a key factor in CaOx nephrolithiasis by multiple studies [10–12]. Another class of metabolites, amino acids, was found to be altered in the urine or blood of nephrolithiasis patients [13,14]. For instance, Gao and others reported that pyroglutamic acid could function as a biomarker for the early diagnosis of nephrolithiasis with urinary metabolomic analysis [14]. Primiano et al. found that urinary amino

* Corresponding author. Department of Urology, Huashan Hospital, Fudan University, Shanghai, 200040, PR China.
** Corresponding author. Department of Urology, Huashan Hospital, Fudan University, Shanghai, 200040, PR China.
E-mail addresses: lukewang2006@126.com (L. Wang), drzhongwu1964@126.com (Z. Wu).
[1] These authors contributed equally to this work.

https://doi.org/10.1016/j.cbi.2023.110570
Received 3 April 2023; Received in revised form 19 May 2023; Accepted 24 May 2023
Available online 25 May 2023

acids were at lower levels in nephrolithiasis patients, including α-aminobutyric acid, isoleucine, methionine, phenylalanine, serine, tryptophan, valine, and else [15]. However, there is limited research on the relationship between bile acids and nephrolithiasis. Bile acids are synthesized in the liver and play a crucial role in digestion and absorption of dietary fats [16]. Some studies suggest that the accumulation of bile acids in the systemic circulation may contribute to endothelial injury in the kidney [17]. One proposed mechanism is that bile acids can cause oxidative stress and inflammation in the kidney, leading to cell damage and impaired renal function [18]. More research is needed to fully understand the relationship between bile acids and nephrolithiasis to develop effective treatments.

Currently, metabolomics has been a growing field of translational research with the potential to recognize biomarkers in the early diagnosis, treatment, and prognostication of kidney diseases such as nephrolithiasis [19–22]. Numerous metabolites and metabolic pathways associated with CaOx nephrolithiasis have been investigated [23–25]. However, most studies focused on the urinary or blood metabolomic profiles and showed the significant disparities in metabolites of CaOx nephrolithiasis patients, likely caused by geographical, ethnic, sampling, and analytical platform differences [26–28]. Therefore, to reduce the interference of extrinsic factors, the metabolomic profiles of well--recognized animal models of CaOx nephrolithiasis are needed to find common and reliable biomarkers.

The rat model for renal CaOx stone formation with ethylene glycol (EG) in free drinking water is a well-established and extensively studied clinical model [29,30]. The administration of EG at appropriate concentrations leads to the accumulation of CaOx on the tubular cell surface, while other metabolic intermediates do not exhibit any toxicity towards renal cells [31]. Thus, our research explored the gut metabolic profiles of rats with 1% EG-induced CaOx nephrolithiasis. After the establishment and evaluation of the CaOx nephrolithiasis rat models, an untargeted metabolomics analysis was applied and the results showed that the bile acids metabolism pathway was significantly altered. Subsequently, the targeted bile acids metabolomics analysis revealed that Hyodeoxycholic acid (HDCA) and Glycohyodeoxycholic acid (GHDCA) significantly increased in CaOx nephrolithiasis models with a biomarker potential. Finally, the network pharmacology results demonstrated that HDCA and GHDCA may act to regulate oxidative stress and apoptotic pathways, which have been reported to be the crucial signaling pathways involved in CaOx nephrolithiasis. In sum, our research displayed intestinal metabolites profiles of EG-induced CaOx nephrolithiasis rats, and we found that bile acids changes, especially HDCA and GHDCA, could be potential biomarkers for CaOx nephrolithiasis.

2. Materials and methods

2.1. EG-induced CaOx nephrolithiasis rat models

Sprague-Dawley (SD) rats (6 weeks old, male) were used to build CaOx nephrolithiasis models and the Fudan Laboratory Animal Ethics Board approved this study. Firstly, 12 SD rats were divided into two equal groups: the control group (named Control) and the model group (named CaOx). Rats in the control group were allowed to drink sterile tap water freely while rats in the model group were administered 1% EG in drinking water for 4 weeks. After 4 weeks, we collected stool samples, blood plasma, ileal and renal tissues. An automatic biochemical analyzer (Servicebio, Wuhan, China) was utilized to analyze renal function, including serum creatinine (Scr), blood urea nitrogen (BUN), and uric acid (UA).

2.2. Histologic analysis

Histologic analysis was used to evaluate the establishment of CaOx nephrolithiasis models. Renal tissues were preserved in 10% formaldehyde, embedded in paraffin, and cut into 5-μm slices for hematoxylin & eosin (H&E), Von Kossa (VK), Periodic Acid-Schiff (PAS), and Masson staining. Terminal deoxynucleotidyl transferase-mediated uridine triphosphate nick end-labeling (TUNEL) staining was performed to label the 3′-end of fragmented DNA in the apoptotic renal tissues, following the manufacturer's instructions (Cat No. C1089, Beyotime, Shanghai, China). For immunofluorescence staining, the ileum sections were incubated overnight at 4 °C with the primary antibody of anti-ZO-1 and anti-Occludin, then continuing to the appropriate secondary antibodies, and concluding with a counterstain of DAPI. Immunohistochemistry (IHC) was conducted to detect nephrolithiasis-related and inflammatory injury protein expression in renal tissues, including CD44, MCP-1, and OPN. The antibodies information (ZO-1, Occludin, CD44, MCP-1, and OPN) are listed in Table S1.

2.3. Real-time quantitative PCR

Total RNA was extracted from kidney and ileum tissues using the RNA extraction kit (Cat No. DP419, Tiangen, Beijing, China) following the manufacturer's instructions. Then, the RNA was reverse-transcribed to synthesize cDNA. Real-time quantitative PCR (RT-qPCR) was performed on a CFX PCR detection system (Bio-Rad, USA) with a SYBR Green kit (Cat No. Q311, Vazyme, Nanjing, China). The primer sequences (CD44, MCP-1, OPN, ZO-1, Occludin, and GAPDH) are also listed in Table S1.

2.4. Untargeted metabolomics

Sample preparation: Stool samples >200 mg were weighed and ground with 5 mm tungsten bead for 1 min at 65 Hz in a Grinding Mill. A mixture of methanol, acetonitrile and water (2:2:1 v/v/v) was precooled to 1 mL and then placed for 1 h of ultrasonic shaking in an ice bath. Afterwards, the mixture was cooled to −20 °C for 1 h, and then centrifuged at 14,000 g for 20 min at 4 °C with collecting supernatants.

LC/MS conditions: Metabolomics profiling was analyzed using a UPLC-ESI-Q-Orbitrap-MS system (UHPLC, Shimadzu Nexera X2 LC-30AD, Shimadzu, Japan) coupled with Q-Exactive Plus (Thermo Scientific, San Jose, USA). For liquid chromatography (LC) separation, samples were analyzed using a ACQUITY UPLC® HSS T3 column (2.1 × 100 mm, 1.8 μm) (Waters, Milford, MA, USA). The flow rate was 0.3 mL/min and the mobile phase contained: A: 0.1% FA in water and B: 100% acetonitrile (ACN). The gradient was 0% buffer B for 2 min and was linearly increased to 48% in 4 min, then up to 100% in 4 min and maintained for 2 min, and then decreased to 0% buffer B in 0.1 min, with 3 min re-equilibration period employed.

ESI-MS/MS Condition: The MS data was acquired using the electrospray ionization (ESI) with both positive and negative modes. The instrument was adjusted to acquire a mass-to-charge range of 70–1050 Da for MS-only acquisition. The resolution of the full MS scans was set to 70,000 at m/z 200, and 17,500 at m/z 200 for MS/MS scans.

2.5. Targeted bile acids metabolomics

Sample preparation: After the stool samples were thawed and smashed, an amount of 0.05 g of the sample was mixed with 500 μL of 70% methanol/water. The sample was vortexed for 3 min under the condition of 2500 r/min and centrifuged at 12000 r/min for 10 min at 4 °C. Take 300 μl of supernatant and refrigerate (−20 °C, 30 min). After the centrifugation at 12000 r/min for 10 min at 4 °C, 200 μl of the supernatant was transferred to a Protein Precipitation Plate for LC-MS analysis.

LC/MS conditions: The analytical conditions were as follows. T3 method: HPLC: column, Waters ACQUITY UPLC HSS T3 C18 (100 mm × 2.1 mm i.d.′1.8 μm); solvent system, water with 0.05% formic acid (A), acetonitrile with 0.05% formic acid (B). The gradient was initiated at 5% B (0 min), increased to 95% B (8–9.5 min) and then returned to 5% B (9.6–12 min). The flow rate was 0.35 mL/min, the temperature was

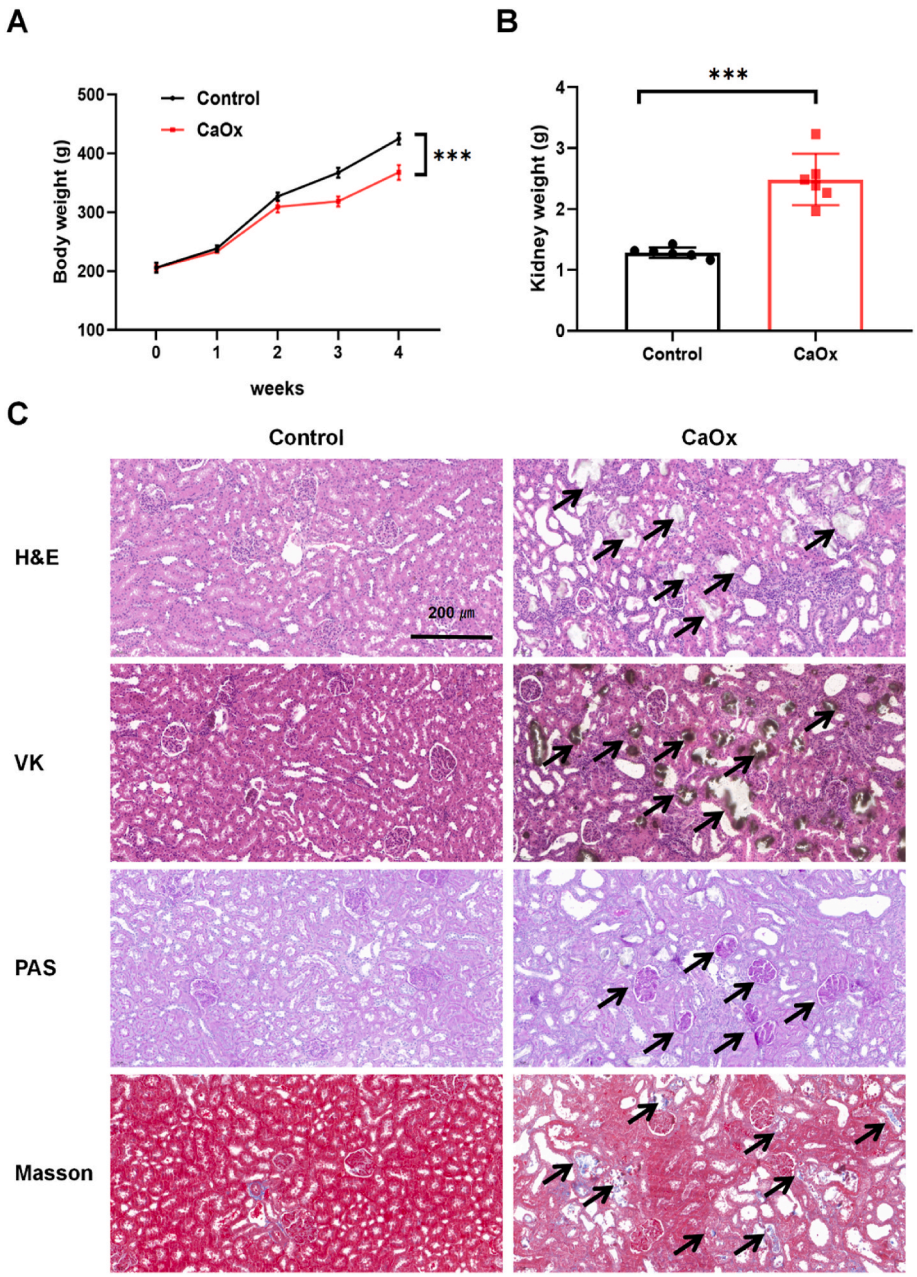

Fig. 1. Evaluation on EG-induced CaOx rat models. **A-B** Body weight (A) and kidney weight (B) of the rats in the control and the CaOx group (n = 6, ***$P < 0.001$). **C** Pathological sections including H&E, VK, PAS, and Masson staining showed the degree of CaOx crystals and kidney injury (magnification × 20; scale bar, 200 μm; arrows in H&E denote crystal formation; arrows in VK denote calcium deposition; arrows in PAS denote renal destructive change; arrows in Masson denote tubulointerstitial fibrosis).

40 °C and the injection volume was 2 μl.

ESI-MS/MS Condition: Linear ion trap (LIT) and triple quadrupole (QQQ) scans were acquired on a triple quadrupole-linear ion trap mass spectrometer (QTRAP), QTRAP® 6500+ LC-MS/MS System, equipped with an ESI Turbo Ion-Spray interface, operating in both positive and negative ion mode. The ESI parameters were set as follows: ion source, ESI+/−; source temperature 550 °C; ion spray voltage (IS) 5500 V (Positive) and −4500 V (Negative); curtain gas (CUR) at 35 psi. Multiple reaction monitoring (MRM) was employed to analyze the metabolites. Mass spectrometer parameters such as declustering potentials (DP) and collision energies (CE) for each MRM transition were optimized using the Multiquant 3.0.3 software (Sciex).

2.6. Predicted target genes and pathways of HDCA and GHDCA in CaOx nephrolithiasis

The molecular structures of HDCA and GHDCA were obtained from PubChem database (https://pubchem.ncbi.nlm.nih.gov/). Then, the SDF files of the 3D structure of HDCA and GHDCA were uploaded to PharmMapper database (http://lilab.ecust.edu.cn/pharmmapper/), to determine the predictive human protein targets related to HDCA and GHDCA. Finally, with UniProt database (https://www.uniprot.org/), the predicted protein lists were converted into the corresponding gene symbols. Thus, a total of 252 target genes of HDCA and GHDCA were selected. Then, CaOx nephrolithiasis-related genes were sourced from GeneCards database (https://www.genecards.org/) and Comparative Toxicogenomics Database (CTD, https://ctdbase.org/). The keywords "calcium oxalate stones" and "calcium oxalate nephrolithiasis" were searched to acquire CaOx nephrolithiasis-related genes. As a result, a total of 370 CaOx nephrolithiasis-related genes were selected from GeneCards database and 108 genes were obtained from CTD database. The Venn diagram displayed the common gene shared in PharmMapper, CTD, and GeneCards; thus, 4 potential target genes (NR1I3, GSR, CASP3, AKT1) of HDCA and GHDCA against CaOx kidney stones were selected. Subsequently, Gene Ontology (GO) and Kyoto Encyclopedia of Genes and Genomes (KEGG) analyses were conducted to explore the potential

Table 1
Biochemical Analysis of the levels of SCr, BUN, UA, and the calcium contents in serum of rats.

Characteristics	Control group (n = 6)	CaOx group (n = 6)	*P* value
Blood urea nitrogen (BUN, mg/dL)	16.8 ± 0.956	41.8 ± 19.8	0.0493*
Serum creatinine (Scr, μmol/L)	33.5 ± 2.64	58.6 ± 12.0	0.0478*
Uric acid (UA, μmol/L)	64.1 ± 2.55	107 ± 34.6	<0.001***
Calcium, (Ca^{2+}, mmol/l)	1.34 ± 0.0331	1.30 ± 0.0132	ns

*$P < 0.05$, ***$P < 0.001$, ns: not significant.

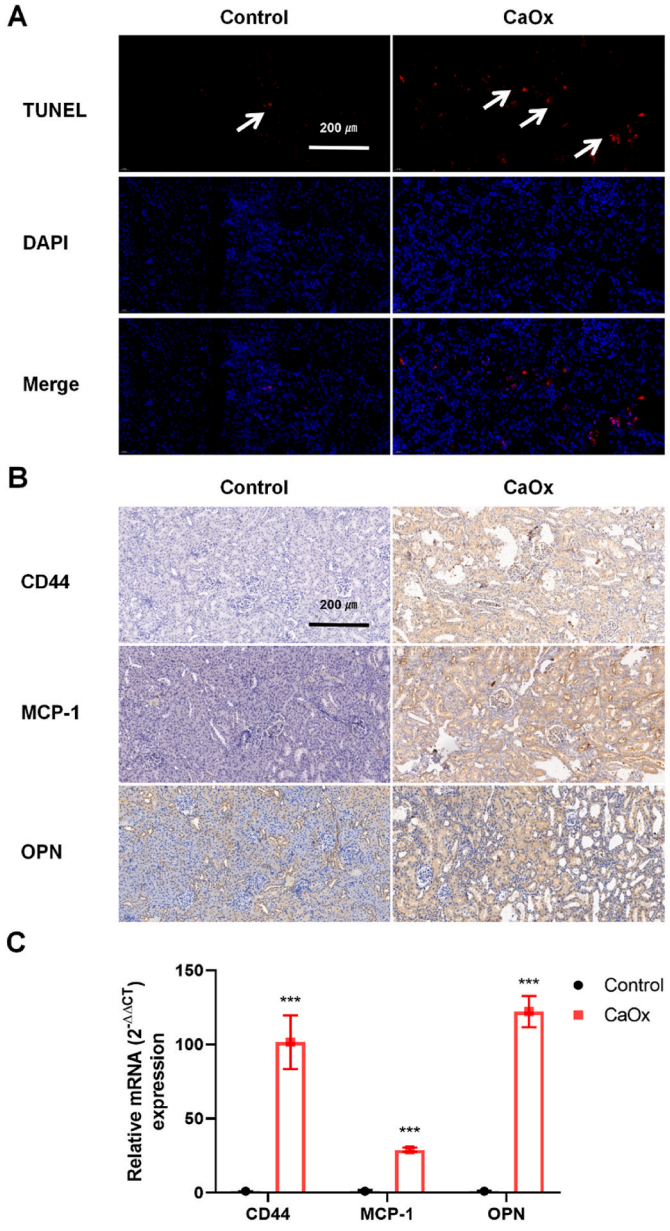

Fig. 2. Apoptosis and inflammation injury in EG-induced CaOx nephrolithiasis rats. **A** Detection of apoptosis in renal tissues with TUNEL assay (magnification × 20; scale bar, 200 μm; arrows denote apoptotic cells). **B** IHC analyses of CD44, MCP-1, and OPN proteins expression in renal tissues (magnification × 20; scale bar, 200 μm). **C** RT-qPCR analyses of CD44, MCP-1, and OPN mRNA expression in renal tissues (mean ± SD, ***$P < 0.001$).

function and signaling pathways of these target genes. GeneMANIA database (http://www.genemania.org/) was utilized to build a PPI network.

2.7. Statistical analysis

R (version 4.0.2) was utilized to conduct all multivariate data analyses and modeling. The data were mean-centered using Pareto scaling. Models were built on principal component analysis (PCA), orthogonal partial least-square discriminant analysis (PLS-DA), partial least-square discriminant analysis (OPLS-DA), and permutation tests (200 permutations) were carried out to prevent overfitting. The discriminating metabolites were obtained using a statistically significant threshold of variable influence on projection (VIP) values obtained from the OPLS-DA model and two-tailed Student's t-test (*P* value) on the normalized raw data at the univariate analysis level. Metabolites with VIP value > 1.0 and *P* value < 0.05 were considered to be statistically significant metabolites by the untargeted metabolomics, and then were subjected to KEGG pathway analysis using the Fisher's exact test with FDR correction, with a nominal statistical significance of $P < 0.05$.

3. Results

3.1. Evaluation on EG-induced CaOx nephrolithiasis rat models

To investigate EG-induced kidney injury and CaOx crystal deposition in rat models, renal function and histopathological changes were detected. The body weight was decreased in the CaOx group (Fig. 1A), but the kidney weight notably increased (Fig. 1B). In addition, the levels of Scr, BUN, and UA in the CaOx group were significantly higher than in the control group. Compared with the control group, CaOx group serum levels of BUN increased from 16.8 ± 0.956 to 41.8 ± 19.8 mg/dl, Scr increased from 33.5 ± 2.64 to 58.6 ± 12.0 μmol/L, and UA increased from 64.1 ± 2.55 to 107 ± 34.6 μmol/L, respectively (Table 1). The serum Ca^{2+} levels did not get a significant difference between the two groups. H&E and VK staining revealed the presence of crystals in the lumen of the renal tubules with tubular dilation in CaOx rats, accompanied by the abnormality of renal histologic structure such as tubular and glomerular atrophy, interstitial inflammation, and loss of brush border (Fig. 1C). Consistently, PAS and Masson staining further revealed the renal injury and interstitial fibrosis in CaOx rats. These findings demonstrate that the models of CaOx were established successfully.

3.2. Inflammation injury and apoptosis in kidneys of EG-induced CaOx nephrolithiasis rat models

The CaOx-mediated apoptosis damage was evaluated through the TUNEL assay (Fig. 2A). The TUNEL staining indicated that the CaOx group had a greater rate of apoptosis of renal tubules compared to the control group. Following, IHC and RT-qPCR analysis showed that the inflammatory injury markers CD44, MCP-1 and OPN expression intensities were upregulated in the kidney of the CaOx group (Fig. 2B and C). These data further prove the effectiveness of CaOx models.

3.3. Intestinal inflammation and permeability in EG-induced CaOx nephrolithiasis rat models

CaOx nephrolithiasis was accompanied by intestinal inflammation and barrier injury, and then intestinal metabolites might mediate the progression of CaOx nephrolithiasis through an impaired gut-kidney axis [32–34]. Therefore, we investigated the intestinal inflammation and permeability in CaOx rats. Histologically, the control group showed intact ileal mucosal architecture, while the CaOx group had inflammation and damage to the intestinal villi with increased numbers of lymphocytes in the lamina propria and epithelium in the ileal tissue (Fig. 3A). In terms of the protein expression of tight junction proteins,

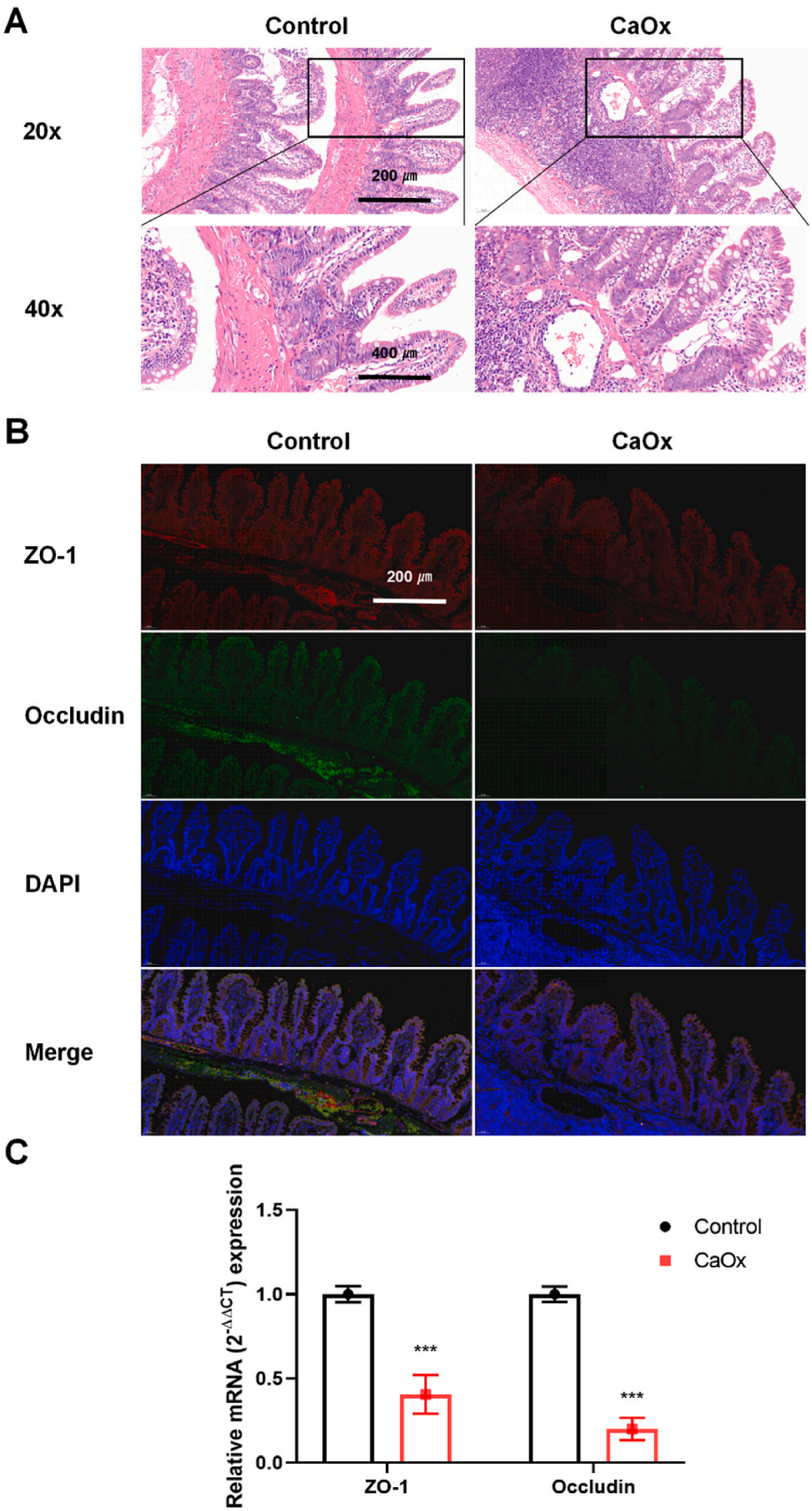

Fig. 3. CaOx-induced intestinal damage. **A** Representative H&E-stained ileum sections images in the control and the CaOx group. **B** The immunofluorescence staining of ZO-1 and Occludin in ileal tissues (magnification × 20; scale bar, 200 μm). **C** RT-qPCR results of ZO-1 and Occludin expression in ileal tissues (mean ± SD, $^{***}P < 0.001$).

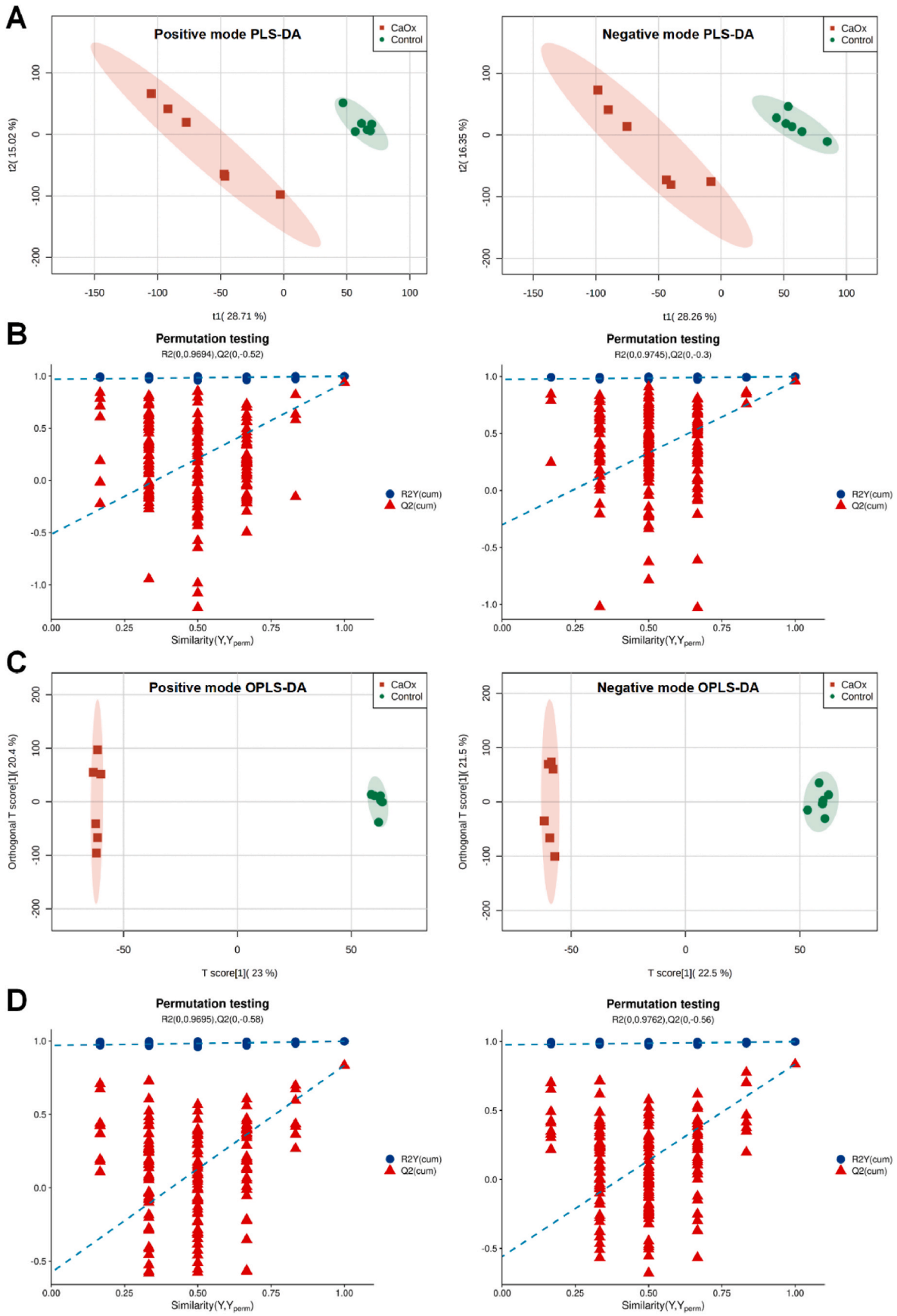

Fig. 4. Distinct metabolic profiles of the CaOx group compared with the control group based on untargeted metabolomics. **A-B** PLS-DA scores (A) and permutation tests (B) in positive and negative ion modes. **C-D** OPLS-DA scores (C) and permutation tests (D) in positive and negative ion modes.

A

Detection mode	Number of DEMs	Up	Down
Postive mode	176	60	116
Negtive mode	93	36	57

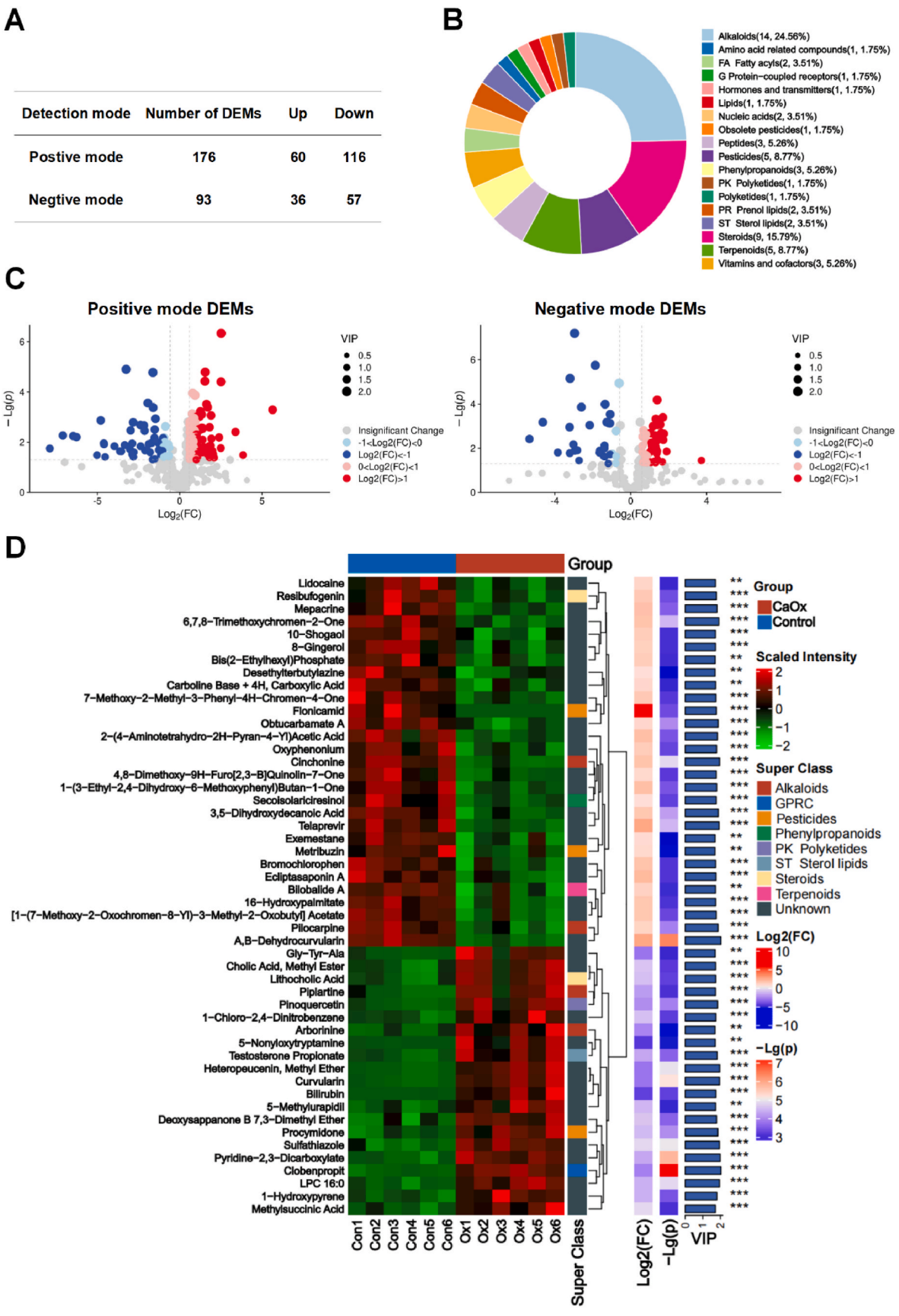

Fig. 5. Differential metabolites (DEMs) between the groups. **A** Statistics of DEMs. **B** KEGG classification of the DEMs. **C** The volcano plot of DEMs between the groups. **D** Complex heatmap of the top 50 DEMs in mixed ion modes.

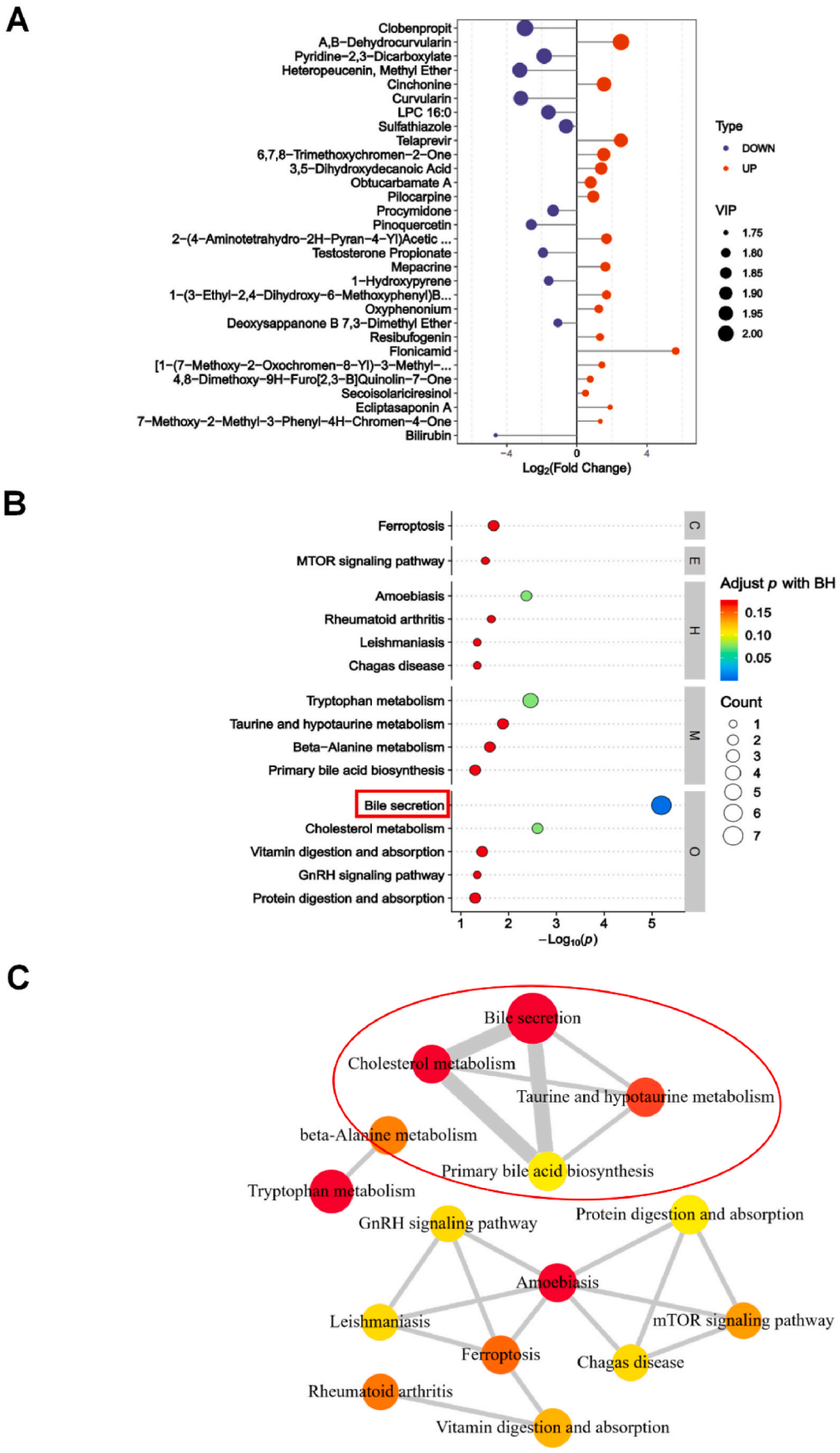

Fig. 6. KEGG analysis of altered metabolites based on the untargeted metabolomics. **A** The top 30 differential metabolites (DEMs) ranked by VIP values were detected in mixed ion modes. **B** KEGG pathway analysis of the top 30 DMEs. **C** Pathways interaction network of KEGG analysis.

ZO-1 and Occludin levels were decreased in the ileal tissues of the CaOx group (Fig. 3B). In agreement with these, the mRNA expression of ZO-1 and Occludin in the CaOx group was also lower than that in the control group (Fig. 3C). These results show that the intestinal barrier was damaged in CaOx rats.

3.4. Untargeted metabolomics profiles

Due to the important role of microbiota and gut-kidney axis in nephrolithiasis, we investigated the levels of intestinal metabolites in rats. The total ion chromatogram of the QC samples revealed that the response intensity and retention time of each chromatographic peak were in agreement, indicating the stability of the instrument and the dependability of the data (Fig. S1A). The PCA plot showed that the QC samples were grouped in both positive and negative ion modes (Fig. S1B). These data suggest that the whole detection process was reliable and the data had a superior quality.

Following, we used PLS-DA and OPLS-DA models to observe the distinction between the two groups. PLS-DA scores unfolded a clear separation in the control group and the CaOx group, both in positive and negative ion modes (Fig. 4A). Permutation analysis validated the PLS-DA model with $R^2Y = 0.998$ and $Q^2 = 0.936$ for positive ion mode and $R^2Y = 0.999$ and $Q^2 = 0.960$ for negative ion mode (Fig. 4B). Consistently, OPLS-DA analysis also showed a substantial separation between the control group and the CaOx group, indicating obvious differences in the untargeted metabolomic profiles (Fig. 4C). Permutation analysis validated the OPLS-DA model with $R^2Y = 0.998$ and $Q^2 = 0.834$ for positive ion mode and $R^2Y = 0.999$ and $Q^2 = 0.836$ for negative ion mode (Fig. 4D). Further details of the permutation analysis of PLS-DA and OPLS-DA were shown in Table S2. According to these results, the model has a good fit degree and prediction ability.

With the cut-off of a VIP >1.0 and $P < 0.05$, differential expression analysis showed that there were 269 significant differential metabolites (DEMs) between the control group and the CaOx group (176 in positive ion modes and 93 in negative ion modes, Fig. 5A). The major metabolite differences were classified by KEGG, including Alkaloids (24.56%), Amino acid-related compounds (1.75%), Fatty acyls (3.51%), G Protein−coupled receptors (1.75%), Hormones and transmitters (1, 1.75%), Lipids (1.75%), Peptides (5.26%), Pesticides (8.77%), and others (Fig. 5B). There were 60 DEMs up-regulated and 116 DEMs down-regulated in the CaOx group in positive ion modes, while there were 36 DEMs up-regulated and 57 DEMs down-regulated in negative ion modes, and the results were depicted as a volcano plot (Fig. 5C). The complex heatmap was constructed to show the top 50 DEMs in mixed ion modes between the two groups (Fig. 5D). This hierarchical cluster analysis showed a significant increase in metabolite levels in the CaOx group, including Gly-Tyr-Ala, Cholic Acid, Methyl Ester Lithocholic Acid, Piplartine and else. **Table S3** provided further details on the DEMs.

3.5. KEGG enrichment analysis

The top 30 DEMs ranked with VIP scores in mixed ion modes (including 3,5−Dihydroxydecanoic Acid, Testosterone Propionate, Heteropeucenin, Curvularin, and other metabolites) were shown in Fig. 6A, indicating their potential to distinguish the CaOx group from the control group. To explore the potential mechanism of CaOx nephrolithiasis, KEGG analysis was conducted to uncover the involved pathways and biological functions of these top 30 DEMs (Fig. 6B). The top 30 DEMs were mainly enriched in bile secretion, cholesterol metabolism, tryptophan metabolism, taurine and hypotaurine metabolism, ferroptosis, vitamin digestion and absorption, primary bile acid biosynthesis, lysine degradation and so on. Furthermore, according to the cut-off of a Benjamini–Hochberg (BH) adjusted filter of $P < 0.05$, the bile secretion pathway was considered as the most significant metabolic pathway, indicating that bile acids metabolism might play a role in CaOx nephrolithiasis. Subsequently, signaling pathways interaction network diagram illustrated the interactions among the four pathways, including bile secretion, cholesterol metabolism, taurine and hypotaurine metabolism, and primary bile acid biosynthesis (Fig. 6C). Further details of the KEGG analysis were shown in Table 2. These results further illustrate the importance of bile acids metabolism in CaOx nephrolithiasis.

Table 2
KEGG pathways of the top 30 DEMs in mix mode based on untargeted metabolomics.

Description	*P* value	*P.* adjust	Q value	RichFactor	TopClass
Bile secretion	<0.001	<0.001	<0.001	9.39	Organismal Systems
Cholesterol metabolism	0.00248	0.0742	0.0613	26.0	Organismal Systems
Tryptophan metabolism	0.00347	0.0742	0.0613	6.27	Metabolism
Amoebiasis	0.00424	0.0742	0.0613	20.0	Human Diseases
Taurine and hypotaurine metabolism	0.0131	0.177	0.146	11.3	Metabolism
Ferroptosis	0.0204	0.177	0.146	8.97	Cellular Processes
Rheumatoid arthritis	0.0229	0.177	0.146	43.4	Human Diseases
beta-Alanine metabolism	0.0246	0.177	0.146	8.13	Metabolism
mTOR signaling pathway	0.0304	0.177	0.146	32.5	Environmental Information Processing
Vitamin digestion and absorption	0.0356	0.177	0.146	6.67	Organismal Systems
GnRH signaling pathway	0.0453	0.177	0.146	21.7	Organismal Systems
Leishmaniasis	0.0453	0.177	0.146	21.7	Human Diseases
Chagas disease	0.0453	0.177	0.146	21.7	Human Diseases
Primary bile acid biosynthesis	0.0499	0.177	0.146	5.54	Metabolism
Protein digestion and absorption	0.0499	0.177	0.146	5.54	Organismal Systems

3.6. Targeted bile acids metabolomics

A total of 30 bile acids were detected by the targeted metabolomics. The overlaid extracted ion current chromatograms (Fig. S2A) and the PCA plot (Fig. S2B) demonstrated the stability and the repeatability of the targeted bile acids metabolomics during this study. Following, the OPLS-DA analysis (Fig. 7A) and permutation analysis (Fig. 7B) showed a substantial separation between the two groups, indicating the obvious differences in the bile acids metabolomic profiles. The list and the detailed results of the bile acids were shown in Table S4.

With the cut-off of a VIP value > 1.0, $P < 0.05$, and $\log_2|\text{fold change}| > 1$, Fig. 7C displayed that there were five significant DEMs between the groups (Nor-Deoxycholic-Acid: Nor-DCA, omega-muricholic-acid: omega-MCA, Hyodeoxycholic-acid: HDCA, Glycohyodeoxycholic-acid: GHDCA, Taurolithocholic-acid: TLCA). Table 3 provided further details on these five significant DEMs based on the targeted bile acid metabolomics. Among these five DEMs, HDCA (VIP = 1.74) and GHDCA (VIP = 1.78) had the highest VIP scores (Fig. 7D). HDCA, GHDCA, and Nor-DCA were up-regulated in the CaOx group, while omega-MCA and TLCA were down-regulated (Fig. 7E). Concurrently, receiver operating characteristic (ROC) analysis was employed to assess the performance of potential biomarkers. HDCA and GHDCA presented the highest predictive accuracy with AUC = 1 to distinct the CaOx group from the control

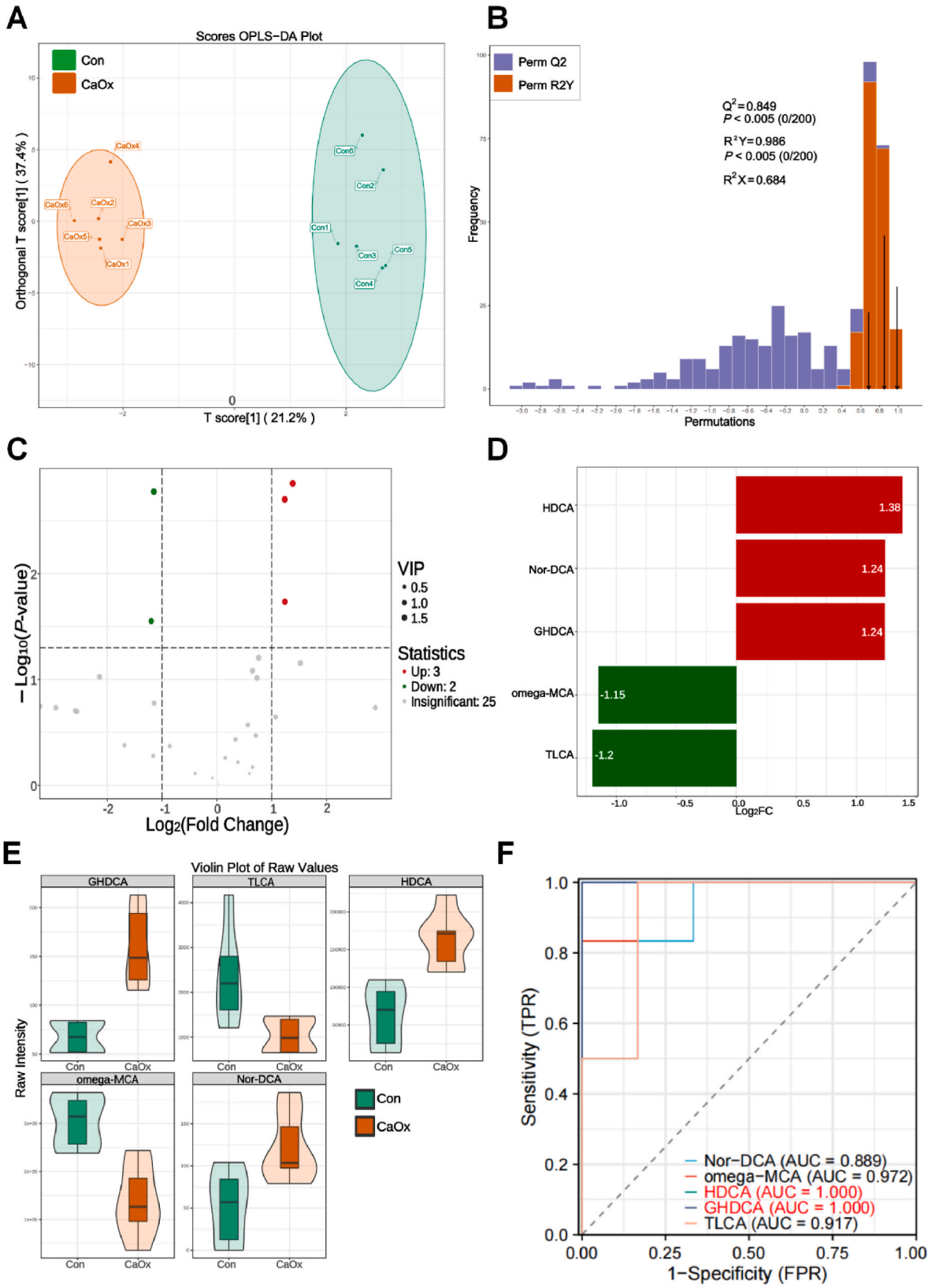

Fig. 7. Distinct bile acids metabolic profiles between the groups based on the targeted metabolomics. **A-B** OPLS-DA score plots (A) and permutation tests (B) of the targeted bile acid metabolomics. **C** The volcano plot of differential metabolites (DEMs) between the groups. **D** The significant differential bile acids ranked by fold change. **E** The abundance of differential bile acids in different groups. **F** Receiver operating characteristic (ROC) analysis of the differential bile acids.

Table 3
The list of the differentially expressed bile acids based on targeted metabolomics.

Compounds	Meanv (Control)	Mean (CaOx)	VIP	*P* value	FC	Type
Nor-Deoxycholic Acid	51.6	122	1.47	0.0184*	2.36	up
omega-muricholic acid	30500	137000	1.72	0.00168**	0.450	down
Hyodeoxycholic acid	62700	164000	1.74	0.00140**	2.61	up
Glycohyodeoxycholic acid	67.5	159	1.78	0.00199**	2.36	up
Taurolithocholic acid	2360	1030	1.54	0.0280*	0.436	down

*$P < 0.05$, **$P < 0.001$, VIP: variable influence on projection, FDR: false discovery rate, FC: fold change.

group (Fig. 7F). This indicates that HDCA and GHDCA might play a crucial role in CaOx nephrolithiasis, but the specific mechanism needs further study.

3.7. Predicted target genes and pathways of HDCA and GHDCA in CaOx nephrolithiasis

Since the high predictive accuracy (AUC = 1) of HDCA and GHDCA in the CaOx group, we explored the potential function of HDCA and GHDCA in CaOx nephrolithiasis with network pharmacology. The 2D molecular structures of HDCA and GHDCA obtained from PubChem database were shown in Fig. 8A and B. Then, a total of 252 common target genes of HDCA and GHDCA were selected from PharmMapper database. Subsequently, we manually identified 370 genes potentially related to CaOx nephrolithiasis with GeneCards database (Table S5) and 108 genes with CTD database (Table S6). Remarkably, to find the key targets of HDCA and GHDCA on CaOx kidney stones, a Venn diagram was acquired by taking the intersection of the target genes of HDCA and GHDCA in PharmMapper, CaOx nephrolithiasis-related genes in CTD and GeneCards. Ultimately, four potential target genes (NR1I3, GSR, CASP3, and AKT1) of HDCA and GHDCA against CaOx nephrolithiasis were selected (Fig. 8C). We further utilized GeneMANIA database to generate a PPI network, and the top 20 genes (APPL1, GSTO2, PHLPP1, ACIN1, PHLPP2 and so on) were presented (Fig. 8D).

Moreover, we performed GO and KEGG analysis to uncover the involved pathways and biological functions of the four target genes of HDCA and GHDCA in CaOx nephrolithiasis (Fig. 8E). The results showed that response to oxidative stress, execution phase of apoptosis, and negative regulation of cell-cell adhesion in biological process (BP), cysteine-type endopeptidase activity involved in apoptotic signaling pathway, and NADP binding were mostly involved in molecular function (MF), mitochondrial matrix and cell-cell junction were enriched in cellular component (CC). Notably, KEGG analysis demonstrated that these target genes were gathered in TNF signaling pathway, apoptosis, and MAPK signaling pathway. As mentioned above, these hub genes were involved in oxidative stress, apoptosis, and cell adhesion, which are vitally significant pathways in the mechanism of kidney stone formation.

4. Discussion

Metabolomics techniques have made great strides in allowing for more precise identification of metabolites connected to nephrolithiasis [35–38]. Denburg et al. identified 18 metabolites that were significantly different between children with CaOx nephrolithiasis and controls, and most of the metabolites that were abundant among those with CaOx nephrolithiasis were classified as amino acids and derivatives [6]. A recent study by Wang reported that arginine was decreased in the ileal contents of the CaOx rat models [39]. Additional studies are needed to address the direct relationship of gut metabolites with CaOx nephrolithiasis progression. Hence, we explored the gut metabolites of CaOx animal models in this study. Firstly, we confirmed that 1% EG-induced CaOx crystal deposition in SD rats was successful. Then, we found an impaired intestinal barrier in the CaOx rat models. The intestinal barrier is essential in safeguarding the body from the detrimental effects of gut microbiota and metabolites; if its function is impaired, it can result in the circulation of hazardous intestinal substances, thus increasing the risk of disease [40]. Therefore, we detected intestinal metabolites by the untargeted and targeted metabolomics, and discovered the differential bile acid metabolites with potential biomarkers in CaOx nephrolithiasis.

With the untargeted metabolomics, we found the main metabolism pathways in CaOx nephrolithiasis, including bile acid metabolism (bile secretion, taurine and hypotaurine metabolism, primary bile acid biosynthesis), and amino acid metabolism (tryptophan metabolism, Beta-Alanine metabolism). Amino acid metabolism is critical for healthy cellular function, metabolism, and growth [41]. As mentioned above, several reports have documented that amino acid metabolites are important in the pathogenesis of nephrolithiasis [42–47]. For example, Hydroxyproline has also been reported to stimulate inflammation and reprogram macrophage signaling in CaOx nephrolithiasis rat models [43]. Glycine has been discovered to suppress kidney calcium oxalate crystal depositions via regulating urinary excretions of oxalate and citrate [44]. L-arginine, which has been reported by multiple groups, may be beneficial in increasing urinary citrate and reducing free radicals in the kidneys of rats *in vivo* and in kidney epithelial cells exposed to oxalate *in vitro* [39,46,47]. However, it is yet to be determined whether these particular metabolites, categories, or pathways are of critical importance in the development of CaOx nephrolithiasis, or if they are simply a consequence.

Bile acids are classical examples of metabolites that are metabolized in the intestine by the gut microbiota into secondary bile acids and therefore emerge as important mediators of metabolic homeostasis [48]. Metabolomics identifies that bile acid changes may serve as biomarkers of metabolic disease such as alcoholic liver disease [49], and hyperuricemia [50]. Whereas, the bile acid metabolism in CaOx nephrolithiasis has been relatively understudied. Tian and others utilized widely targeted metabolomics analysis in rats and found that secondary bile acid pathways may influence CaOx nephrolithiasis [45]. Another metabolomics analysis demonstrated that two conjugated bile acids, taurocholic acid and taurodeoxycholic acid, were significantly decreased in hydroxy-L-proline-induced CaOx nephrolithiasis rats [36]. Similarly, in this research, two conjugated bile acids, omega-MCA and TLCA were observed down-regulated in the CaOx nephrolithiasis group. It has been suggested that unabsorbed bile acids and fatty acids will combine with intestinal calcium to create saponification and then reduce the binding between free calcium and oxalate in the intestinal lumen, thus increasing intestinal oxalate absorption and hyperoxaluria [51]. Also, unabsorbed bile salts and fatty acids increase colonic permeability, the site of oxalate hyper-absorption in enteric hyperoxaluria [52]. Consistently, with the targeted bile acids metabolomics, we discovered that Nor-DCA, HDCA, GHDCA were up-regulated in the CaOx nephrolithiasis group. Notably, HDCA and GHDCA held strong predictive power with AUC = 1. Very few studies have been done on GHDCA. In terms of HDCA, contrasting results have been reported. Previous studies have reported that the increased HDCA may have glucose-lowering effects and exert an anti-inflammatory effect on colitis by downregulating inflammatory cytokines [53]. Despite these potential benefits, their practical application is likely to be limited due to the damaging effects of CaOx, and the high cytotoxicity of HDCA was reported as well [54]. Following, the level of HDCA was observed to increase significantly in

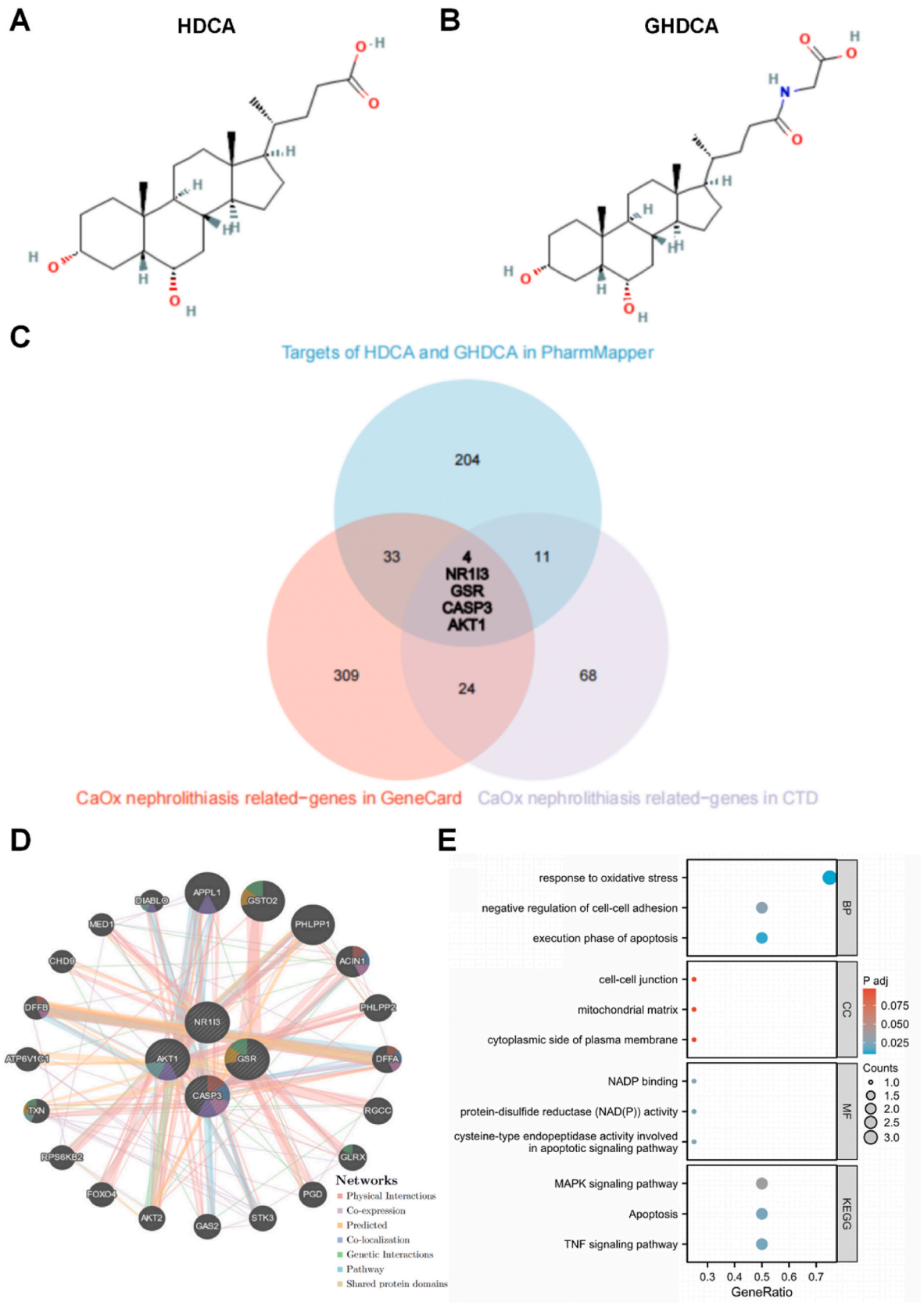

Fig. 8. Predicted target genes and pathways of HDCA and GHDCA in CaOx nephrolithiasis. **A** HDCA and GHDCA molecular structures obtained from PubChem database. **B** Venn diagram was acquired by taking the intersection of the targets of HDCA and GHDCA in PharmMapper, the CaOx nephrolithiasis-related genes in CTD and GeneCards databases. **C** The PPI network of HDCA and GHDCA target genes via GeneMANIA database. **D** GO and KEGG enrichment analysis of HDCA and GHDCA target genes in CaOx nephrolithiasis.

severe enteropathy like ulcerative colitis [55,56] and in ketorolac-induced dysbiosis [57]. These data suggest the complex role of HDCA in different diseases.

Finally, we preliminarily explored the pathway of HDCA and GHDCA in CaOx nephrolithiasis. The formation of kidney stones in humans is caused by oxalate-induced damage and the accumulation of CaOx crystals and their subsequent adherence while it is currently accepted that oxidative stress is a trigger and regulator of apoptosis and inflammation, then leading to renal tubular damage, as well as the attachment and accumulation of CaOx crystals [58,59]. Consistently, with the network pharmacology analysis, we found the possible regulatory mechanism of HDCA and GHDCA in CaOx nephrolithiasis, including oxidative stress accompanying modulation of apoptosis.

Attention is growing to the application of metabolomics. However, few studies have been conducted on the role of gut bile acids metabolites in CaOx nephrolithiasis. Our research provides insight into the role and potential mechanism of bile acid metabolites in CaOx nephrolithiasis. To the best of our knowledge, none of the previous urolithiasis studies has reported on the bile acid profiles in CaOx nephrolithiasis utilizing the untargeted and targeted metabolomics. The novel metabolites may also help understand the association between gut dysbiosis and CaOx kidney stones [60,61]. In the follow-up experiment, the association between gut flora and the DEMs identified in this study will be further explored.

EG exposure through drinking water in Wistar or SD rats is a widely used animal model for studying hyperoxaluria and CaOx nephrolithiasis. However, this approach has been criticized due to the nephrotoxicity of EG and some of its metabolites, as well as the metabolic acidosis caused by EG Ref. [62]. In fact, many of the global metabolic changes could be, due to chronic EG administration and have a likelihood of not being present in idiopathic CaOx nephrolithiasis. Chronic EG administration, typically seen in cases of EG poisoning, can lead to several metabolic changes in the body [63]. EG is primarily metabolized in the liver through several enzymatic reactions, which produce toxic metabolites that can affect various organs and systems, including glycolic acid and oxalic acid [64]. These metabolic byproducts can contribute to metabolic acidosis, kidney damage, and calcium oxalate crystal formation in the urinary system. As a result, it becomes challenging to distinguish the effects of EG and its metabolites from those induced by CaOx crystals. Therefore, there are limitations in this research: (1) the EG-induced CaOx rat models cannot adequately mimic the development of CaOx nephrolithiasis. Thus, the studies on other CaOx nephrolithiasis animal models and patients with bigger sample and multicenter are warranted. (2) the specific function and mechanism of HDCA and GHDCA in CaOx nephrolithiasis are still needed to be explored *in vivo* and *in vitro*. (3) follow-up studies are needed to investigate the levels of the metabolites in the blood and urine.

5. Conclusion

In conclusion, we identified potential biomarkers, bile acid metabolites, in CaOx nephrolithiasis rat models with the untargeted and targeted metabolomics, a developing technology that is playing a key role in comprehending health and disease states with the potential to improve diagnosis and treatment of CaOx nephrolithiasis. Thus, our findings provide a diagnostic basis for pre-clinical studies of bile acids as potential biomarkers for CaOx nephrolithiasis.

Author statement

ZZJ: Conceptualization, methodology, formal analysis, visualization, writing-original draft; FDX: Formal analysis, methodology; SDH: Formal analysis, supervision; GP: Formal analysis; WLJ: Formal analysis, supervision, funding acquisition; WZ: Writing-review & editing, conceptualization, supervision, funding acquisition.

Declaration of competing interest

The authors declare that they have no known competing financial interests or personal relationships that could have appeared to influence the work reported in this paper.

Data availability

Data will be made available on request.

Acknowledgements

This research was funded by National Natural Science Foundation of China (No. 81970603 and No. 82100807).

Appendix A. Supplementary data

Supplementary data to this article can be found online at https://doi.org/10.1016/j.cbi.2023.110570.

References

[1] T. Knoll, A.B. Schubert, D. Fahlenkamp, D.B. Leusmann, G. Wendt-Nordahl, G. Schubert, Urolithiasis through the ages: data on more than 200,000 urinary stone analyses, J. Urol. 185 (2011) 1304–1311.
[2] M.Q. Fakhoury, B. Gordon, B. Shorter, A. Renson, M.S. Borofsky, M.R. Cohn, E. Cabezon, J.S. Wysock, M.A. Bjurlin, Perceptions of dietary factors promoting and preventing nephrolithiasis: a cross-sectional survey, World J. Urol. 37 (2019) 1723–1731.
[3] A.L. Zisman, F.L. Coe, A.J. Cohen, C.B. Riedinger, E.M. Worcester, Racial differences in risk factors for kidney stone formation, Clin. J. Am. Soc. Nephrol. : CJASN 15 (2020) 1166–1173.
[4] C. Witting, C.B. Langman, D. Assimos, M.A. Baum, A. Kausz, D. Milliner, G. Tasian, E. Worcester, M. Allain, M. West, F. Knauf, J.C. Lieske, Pathophysiology and treatment of enteric hyperoxaluria, Clin. J. Am. Soc. Nephrol. : CJASN 16 (2021) 487–495.
[5] S.M.-W. Yu, J.C. He, Happy gut, happy kidneys? Restoration of gut microbiome ameliorates acute and chronic kidney disease, Cell Metabol. 33 (2021) 1901–1903.
[6] M.R. Denburg, K. Koepsell, J.J. Lee, J. Gerber, K. Bittinger, G.E. Tasian, Perturbations of the gut microbiome and metabolome in children with calcium oxalate kidney stone disease, J. Am. Soc. Nephrol. : JASN (J. Am. Soc. Nephrol.) 31 (2020) 1358–1369.
[7] Y. Yang, S. Hong, J. Xu, C. Li, S. Wang, Y. Xun, Enterobacter cloacae: a villain in CaOx stone disease? Urolithiasis 50 (2022) 177–188.
[8] S.Y. Hong, Y.Y. Yang, J.Z. Xu, Q.D. Xia, S.G. Wang, Y. Xun, The renal pelvis urobiome in the unilateral kidney stone patients revealed by 2bRAD-M, J. Transl. Med. 20 (2022) 431.
[9] J. Gao, N. Zhou, Y. Wu, M. Lu, Q. Wang, C. Xia, M. Zhou, Y. Xu, Urinary metabolomic changes and microbiotic alterations in presenilin1/2 conditional double knockout mice, J. Transl. Med. 19 (2021) 351.
[10] Y. Liu, X. Jin, Y. Ma, Z. Jian, Z. Wei, L. Xiang, Q. Sun, S. Qi, K. Wang, H. Li, Short-Chain Fatty Acids Reduced Renal Calcium Oxalate Stones by Regulating the Expression of Intestinal Oxalate Transporter SLC26A6, mSystems, 2021, e0104521.
[11] Y. Liu, X. Jin, H.G. Hong, L. Xiang, Q. Jiang, Y. Ma, Z. Chen, L. Cheng, Z. Jian, Z. Wei, J. Ai, S. Qi, Q. Sun, H. Li, Y. Li, K. Wang, The relationship between gut microbiota and short chain fatty acids in the renal calcium oxalate stones disease, Faseb. J. 34 (2020) 11200–11214.
[12] H.X. Du, S.Y. Yue, D. Niu, C. Liu, L.G. Zhang, J. Chen, Y. Chen, Y. Guan, X.L. Hua, C. Li, X.G. Chen, L. Zhang, C.Z. Liang, Gut microflora modulates Th17/treg cell differentiation in experimental autoimmune prostatitis via the short-chain fatty acid propionate, Front. Immunol. 13 (2022), 915218.
[13] J.D. Rimer, A.M. Kolbach-Mandel, M.D. Ward, J.A. Wesson, The role of macromolecules in the formation of kidney stones, Urolithiasis 45 (2017) 57–74.
[14] H. Gao, J. Lin, F. Xiong, Z. Yu, S. Pan, Y. Huang, Urinary microbial and metabolomic profiles in kidney stone disease, Front. Cell. Infect. Microbiol. 12 (2022), 953392.
[15] A. Primiano, S. Persichilli, P.M. Ferraro, R. Calvani, A. Biancolillo, F. Marini, A. Picca, E. Marzetti, A. Urbani, J. Gervasoni, A specific urinary amino acid profile characterizes people with kidney stones, Dis. Markers 2020 (2020), 8848225.
[16] M.J. Monte, J.J. Marin, A. Antelo, J. Vazquez-Tato, Bile acids: chemistry, physiology, and pathophysiology, World J. Gastroenterol. 15 (2009) 804–816.
[17] M.J. Perez, O. Briz, Bile-acid-induced cell injury and protection, World J. Gastroenterol. 15 (2009) 1677–1689.
[18] A. Bomzon, S. Holt, K. Moore, Bile acids, oxidative stress, and renal function in biliary obstruction, Semin. Nephrol. 17 (1997) 549–562.
[19] A. Metwaly, S. Reitmeier, D. Haller, Microbiome risk profiles as biomarkers for inflammatory and metabolic disorders, Nat. Rev. Gastroenterol. Hepatol. 19 (2022) 383–397.

[20] P.R. Pereira, D.F. Carrageta, P.F. Oliveira, A. Rodrigues, M.G. Alves, M. P. Monteiro, Metabolomics as a tool for the early diagnosis and prognosis of diabetic kidney disease, Med. Res. Rev. 42 (2022) 1518–1544.
[21] J.I. Martínez-Montoro, E. Morales, I. Cornejo-Pareja, F.J. Tinahones, J. C. Fernández-García, Obesity-related glomerulopathy: current approaches and future perspectives, Obes. Rev. : Off. J. Int. Assoc. Study Obes. 23 (2022), e13450.
[22] B.H. Banimfreg, H. Alshraideh, A. Shamayleh, A. Guella, M.H. Semreen, M.T. Al Bataineh, N.C. Soares, Untargeted metabolomic plasma profiling of Emirati dialysis patients with diabetes versus non-diabetic: a pilot study, Biomolecules 12 (2022).
[23] D.E. Jewell, S.K. Tavener, R.L. Hollar, K.S. Panickar, Metabolomic changes in cats with renal disease and calcium oxalate uroliths, Metabolomics, Off. J. Metabol. Soc. 18 (2022) 68.
[24] C. Thongprayoon, I. Vuckovic, L.E. Vaughan, S. Macura, N.B. Larson, et al., Nuclear Magnetic Resonance Metabolomic Profiling and Urine Chemistries in Incident Kidney Stone Formers Compared with Controls, Journal of the American Society of Nephrology : JASN 33 (2022) 2071–2086.
[25] M.M. Tsamouri, B.P. Durbin-Johnson, W.T.N. Culp, C.A. Palm, M. Parikh, M. S. Kent, P.M. Ghosh, Untargeted metabolomics identify a panel of urinary biomarkers for the diagnosis of urothelial carcinoma of the bladder, as compared to urolithiasis with or without urinary tract infection in dogs, Metabolites (2022) 12.
[26] X. Wang, M. Wang, J. Ruan, S. Zhao, J. Xiao, Y. Tian, Identification of urine biomarkers for calcium-oxalate urolithiasis in adults based on UPLC-Q-TOF/MS, J. Chromatogr., B: Anal. Technol. Biomed. Life Sci. 1124 (2019) 290–297.
[27] L. Shavit, P.M. Ferraro, N. Johri, W. Robertson, S.B. Walsh, S. Moochhala, R. Unwin, Effect of being overweight on urinary metabolic risk factors for kidney stone formation, Nephrol. Dial. Transplant. 30 (2015) 607–613, official publication of the European Dialysis and Transplant Association - European Renal Association.
[28] J. Wen, Y. Cao, Y. Li, F. Zhu, M. Yuan, J. Xu, J. Li, Metabolomics analysis of the serum from children with urolithiasis using UPLC-MS, Clin. Transl. Sci. 14 (2021) 1327–1337.
[29] A. Okada, S. Nomura, Y. Higashibata, M. Hirose, B. Gao, M. Yoshimura, Y. Itoh, T. Yasui, K. Tozawa, K. Kohri, Successful formation of calcium oxalate crystal deposition in mouse kidney by intraabdominal glyoxylate injection, Urol. Res. 35 (2007) 89–99.
[30] K. McMartin, Are calcium oxalate crystals involved in the mechanism of acute renal failure in ethylene glycol poisoning? Clin. Toxicol. 47 (2009) 859–869.
[31] G. Anan, T. Hirose, D. Kikuchi, C. Takahashi, A. Endo, H. Ito, S. Sato, S. Nakayama, H. Hashimoto, K. Ishiyama, T. Kimura, K. Takahashi, M. Sato, T. Mori, Inhibition of sodium-glucose cotransporter 2 suppresses renal stone formation, Pharmacol. Res. 186 (2022), 106524.
[32] Y.-Y. Chen, D.-Q. Chen, L. Chen, J.-R. Liu, N.D. Vaziri, Y. Guo, Y.-Y. Zhao, Microbiome-metabolome reveals the contribution of gut-kidney axis on kidney disease, J. Transl. Med. 17 (2019) 5.
[33] S. Robijn, B. Hoppe, B.A. Vervaet, P.C. D'Haese, A. Verhulst, Hyperoxaluria: a gut-kidney axis? Kidney Int. 80 (2011) 1146–1158.
[34] A. Ticinesi, A. Nouvenne, G. Chiussi, G. Castaldo, A. Guerra, T. Meschi, Calcium oxalate nephrolithiasis and gut microbiota: not just a gut-kidney Axis. A nutritional perspective, Nutrients 12 (2020).
[35] X. Xu, J. Chen, H. Lv, Y. Xi, A. Ying, X. Hu, Molecular mechanism of Pyrrosia lingua in the treatment of nephrolithiasis: network pharmacology analysis and in vivo experimental verification, Phytomedicine 98 (2022), 153929.
[36] S. Gao, R. Yang, Z. Peng, H. Lu, N. Li, J. Ding, X. Cui, W. Chen, X. Dong, Metabolomics analysis for hydroxy-L-proline-induced calcium oxalate nephrolithiasis in rats based on ultra-high performance liquid chromatography quadrupole time-of-flight mass spectrometry, Sci. Rep. 6 (2016), 30142.
[37] X. Duan, T. Zhang, L. Ou, Z. Kong, W. Wu, G. Zeng, (1)H NMR-based metabolomic study of metabolic profiling for the urine of kidney stone patients, Urolithiasis 48 (2020) 27–35.
[38] M.L. Ellis, K.J. Shaw, S.B. Jackson, S.L. Daniel, J. Knight, Analysis of commercial kidney stone probiotic supplements, Urology 85 (2015) 517–521.
[39] Y. Liu, X. Jin, L. Tian, Z. Jian, Y. Ma, L. Cheng, Y. Cui, H. Li, Q. Sun, K. Wang, Lactiplantibacillus plantarum reduced renal calcium oxalate stones by regulating arginine metabolism in gut microbiota, Front. Microbiol. 12 (2021), 743097.
[40] R. Wang, X. Yang, J. Liu, F. Zhong, C. Zhang, Y. Chen, T. Sun, C. Ji, D. Ma, Gut microbiota regulates acute myeloid leukaemia via alteration of intestinal barrier function mediated by butyrate, Nat. Commun. 13 (2022) 2522.
[41] X. Li, S. Zheng, G. Wu, Amino acid metabolism in the kidneys: nutritional and physiological significance, Adv. Exp. Med. Biol. 1265 (2020) 71–95.
[42] S. Farmanesh, J. Chung, R.D. Sosa, J.H. Kwak, P. Karande, J.D. Rimer, Natural promoters of calcium oxalate monohydrate crystallization, J. Am. Chem. Soc. 136 (2014) 12648–12657.
[43] P. Kumar, Z. Yang, J.M. Lever, M.D. Chávez, H. Fatima, D.K. Crossman, C. L. Maynard, J.F. George, T. Mitchell, Hydroxyproline stimulates inflammation and reprograms macrophage signaling in a rat kidney stone model, Biochimica et biophysica acta, Mol. Basis Dis. 1868 (2022), 166442.
[44] Y. Lan, W. Zhu, X. Duan, T. Deng, S. Li, Y. Liu, Z. Yang, Y. Wen, L. Luo, S. Zhao, J. Wang, Z. Zhao, W. Wu, G. Zeng, Glycine suppresses kidney calcium oxalate crystal depositions via regulating urinary excretions of oxalate and citrate, J. Cell. Physiol. 236 (2021) 6824–6835.
[45] L. Tian, Y. Liu, X. Xu, P. Jiao, G. Hu, Y. Cui, J. Chen, Y. Ma, X. Jin, K. Wang, Q. Sun, Lactiplantibacillus plantarum J-15 reduced calcium oxalate kidney stones by regulating intestinal microbiota, metabolism, and inflammation in rats, Faseb. J. 36 (2022), e22340.
[46] A.D. Kandhare, M.V. Patil, S.L. Bodhankar, L-Arginine attenuates the ethylene glycol induced urolithiasis in ininephrectomized hypertensive rats: role of KIM-1, NGAL, and NOs, Ren. Fail. 37 (2015) 709–721.
[47] T. Kizivat, M. Smolić, I. Marić, M. Tolušić Levak, R. Smolić, I. Bilić Ćurčić, L. Kuna, I. Mihaljević, A. Včev, S. Tucak-Zorić, Antioxidant pre-treatment reduces the toxic effects of oxalate on renal epithelial cells in a cell culture model of urolithiasis, Int. J. Environ. Res. Publ. Health 14 (2017).
[48] M. Li, T. Liu, T. Yang, J. Zhu, Y. Zhou, M. Wang, Q. Wang, Gut microbiota dysbiosis involves in host non-alcoholic fatty liver disease upon pyrethroid pesticide exposure, Environ. Sci. Ecotechnol. 11 (2022), 100185.
[49] G. Charkoftaki, W.Y. Tan, P. Berrios-Carcamo, D.J. Orlicky, J.P. Golla, R. Garcia-Milian, R. Aalizadeh, N.S. Thomaidis, D.C. Thompson, V. Vasiliou, Liver metabolomics identifies bile acid profile changes at early stages of alcoholic liver disease in mice, Chem. Biol. Interact. 360 (2022), 109931.
[50] Y. Chen, C. Pei, Y. Chen, X. Xiao, X. Zhang, K. Cai, S. Deng, R. Liang, Z. Xie, P. Li, Q. Liao, Kidney tea ameliorates hyperuricemia in mice via altering gut microbiota and restoring metabolic profile, Chem. Biol. Interact. 376 (2023), 110449.
[51] R.R. Ferraz, H.G. Tiselius, I.P. Heilberg, Fat malabsorption induced by gastrointestinal lipase inhibitor leads to an increase in urinary oxalate excretion, Kidney Int. 66 (2004) 676–682.
[52] J.R. Asplin, The management of patients with enteric hyperoxaluria, Urolithiasis 44 (2016) 33–43.
[53] D.M. Shih, Z. Shaposhnik, Y. Meng, M. Rosales, X. Wang, J. Wu, B. Ratiner, F. Zadini, G. Zadini, A.J. Lusis, Hyodeoxycholic acid improves HDL function and inhibits atherosclerotic lesion formation in LDLR-knockout mice, Faseb. J. 27 (2013) 3805–3817.
[54] Y. Araki, T. Tsujikawa, A. Andoh, M. Sasaki, Y. Fujiyama, T. Bamba, Therapeutic effects of an oral adsorbent on acute dextran sulphate sodium-induced colitis and its recovery phase in rats, especially effects of elimination of bile acids in gut lumen, Digestive and liver disease, Off. J. Ital. Soc. Gastroenterol. Ital. Assoc. Study Liver 32 (2000) 691–698.
[55] F. Liu, X. Wang, D. Li, Y. Cui, X. Li, Apple polyphenols extract alleviated dextran sulfate sodium-induced ulcerative colitis in C57BL/6 male mice by restoring bile acid metabolism disorder and gut microbiota dysbiosis, Phytother Res. : PT 35 (2021) 1468–1485.
[56] C. Gnewuch, G. Liebisch, T. Langmann, B. Dieplinger, T. Mueller, M. Haltmayer, H. Dieplinger, A. Zahn, W. Stremmel, G. Rogler, G. Schmitz, Serum bile acid profiling reflects enterohepatic detoxification state and intestinal barrier function in inflammatory bowel disease, World J. Gastroenterol. 15 (2009) 3134–3141.
[57] B. Hutka, B. Lázár, A.S. Tóth, B. Ágg, S.B. László, N. Makra, B. Ligeti, B. Scheich, K. Király, M. Al-Khrasani, D. Szabó, P. Ferdinandy, K. Gyires, Z.S. Zádori, The nonsteroidal anti-inflammatory drug ketorolac alters the small intestinal microbiota and bile acids without inducing intestinal damage or delaying peristalsis in the rat, Front. Pharmacol. 12 (2021), 664177.
[58] A.P. Evan, E.M. Worcester, F.L. Coe, J. Williams Jr., J.E. Lingeman, Mechanisms of human kidney stone formation, Urolithiasis 43 (Suppl 1) (2015) 19–32.
[59] S.R. Khan, M.S. Pearle, W.G. Robertson, G. Gambaro, B.K. Canales, S. Doizi, O. Traxer, H.G. Tiselius, Kidney stones, Nat. Rev. Dis. Prim. 2 (2016), 16008.
[60] H. Zhao, X. Chen, L. Zhang, F. Meng, L. Zhou, X. Pang, Z. Lu, Y. Lu, Lacticaseibacillus rhamnosus Fmb14 prevents purine induced hyperuricemia and alleviate renal fibrosis through gut-kidney axis, Pharmacol. Res. 182 (2022), 106350.
[61] X. Jin, Z. Jian, X. Chen, Y. Ma, H. Ma, Y. Liu, L. Gong, L. Xiang, S. Zhu, X. Shu, S. Qi, H. Li, K. Wang, Short chain fatty acids prevent glyoxylate-induced calcium oxalate stones by GPR43-dependent immunomodulatory mechanism, Front. Immunol. 12 (2021), 729382.
[62] S.R. Khan, P.A. Glenton, K.J. Byer, Modeling of hyperoxaluric calcium oxalate nephrolithiasis: experimental induction of hyperoxaluria by hydroxy-L-proline, Kidney Int. 70 (2006) 914–923.
[63] J.S. LaKind, E.A. McKenna, R.P. Hubner, R.G. Tardiff, A review of the comparative mammalian toxicity of ethylene glycol and propylene glycol, Crit. Rev. Toxicol. 29 (1999) 331–365.
[64] R.A. Corley, M.E. Meek, E.W. Carney, Mode of action: oxalate crystal-induced renal tubule degeneration and glycolic acid-induced dysmorphogenesis–renal and developmental effects of ethylene glycol, Crit. Rev. Toxicol. 35 (2005) 691–702.